Theoretical study of fluorine doping in layered LaOBiS_{2}-type compounds

Naomi Hirayama, Masayuki Ochi, and Kazuhiko Kuroki

Phys. Rev. B **100**, 125201 — Published 5 September 2019

DOI: 10.1103/PhysRevB.100.125201

Theoretical Study of Fluorine Doping in Layered $LaOBiS_2$-type Compounds

Naomi Hirayama*, Masayuki Ochi, and Kazuhiko Kuroki

Osaka University, 1-1 Machikaneyama-cho, Toyonaka-shi, Osaka 560-0043, Japan

*E-mail: hirayama@presto.phys.sci.osaka-u.ac.jp

ABSTRACT

We theoretically investigate the fluorine doping in $LaOBiS_2$-type quaternary compounds ($LaOBiS_2$, $NdOBiS_2$, $LaOBiSe_2$, and $LaOSbSe_2$), which are promising candidates of thermoelectric and superconducting materials. These compounds possess a layered structure comprising blocking *Ln*O (*Ln* = La, Nd, etc.) layers and conducting $PnCh_2$ (*Pn* = Bi, Sb; *Ch* = S, Se) layers. Their carrier concentration is generally tuned via substitutional doping of F atoms in the O site for improving the thermoelectric performance or the superconductivity; however, the tunability of the electrical properties via F doping strongly depends on constituent elements. In order to elucidate the difference, we theoretically examine the electronic and structural properties of these F-doped systems using first-principles calculation. Our results show that the monoclinic distortion of the mother compound, which is closely related to the *Pn* element, can drastically decrease the capability of F doping. Replacement of the *Ln* atom from La to Nd in $LnOBiS_2$ makes F doping difficult, which is consistent with experimental observation. We also find that the tetragonal structure is gradually stabilized by F-doping for all the systems investigated in this study. Our results will be important knowledge for controlling the electrical properties of $LaOBiS_2$-type compounds both as thermoelectric and superconducting materials.

I. INTRODUCTION

Materials science for solving the energy problem is nowadays of crucial importance. To this end, several technologies have been actively developed such as the thermoelectric effects, the direct conversion between thermal and electric energy, and the superconductivity, which enables efficient power transmission. For these technologies, efficient thermoelectric conversion enabled by a high value of the dimensionless figure of merit (*ZT*) and high superconducting transition temperature are the central objectives, respectively, for which materials search has been conducted by many researchers. In such materials search, the controllability of the carrier concentration is often an essential aspect of candidate materials to optimize their functionalities.

$LaOBiS_2$,[1] which comprises blocking LaO layers and conducting BiS_2 layers, has attracted much attention as superconducting[2-10] and thermoelectric[11-18] material. One of the remarkable features of this material is a relatively low thermal conductivity, ~2 W m^{-1} K^{-1} at room temperature,[19] which is advantageous for increasing *ZT*. Another important characteristic is a rich variety of constituent elements. For example, a capability of substitution of F atoms with O atoms in LaO layers offers high controllability of carrier concentration. Since $LaOBiS_2$ has a large band gap without doping carriers,[20, 21] the capability of the carrier doping is indispensable for employing it as superconducting or thermoelectric materials. For instance, high superconducting transition temperature was observed in $LaO_{1-x}F_xBiS_2$ with $x = 0.5$.[1] Also, the thermoelectric performance of $LaOBiS_2$ can be improved by utilizing the large degrees of freedom of constituent elements not limited to O atoms. An experimental study revealed that the thermoelectric performance can be improved by partial replacement of S atoms with Se atoms, where $ZT = 0.17$ at 723 K is realized in $LaOBiS_{2-x}Se_x$ with $x = 0.8$.[19] A further high *ZT* of approximately 0.36 with low thermal conductivity of 0.8—1.2 W m^{-1} K^{-1} at around 650 K was achieved in a densified sample of LaOBiSSe.[22] It was also shown that the Se substitution reduces the lattice thermal conductivity by softening the rattling phonon modes in $LaOBiS_{2-x}Se_x$.[15] In addition, a theoretical study[23]

predicted that replacing Bi with Sb or As together with replacing S with Se can considerably improve the power factor of this compound. From this viewpoint, a recent experimental study that reported a successful synthesis of *Ln*OSbSe$_2$ (*Ln* = La, Ce) is intriguing.[24] While low thermal conductivity of 1.5 and 0.8 W m^{-1} K^{-1} at room temperature were found for *Ln* = La and Ce, respectively, there remains a difficulty in lowering their high electrical resistivity, which was also reported in Ce(O,F)SbS$_2$.[25] Although a recent experimental study on $NdO_{0.8}F_{0.2}Sb_{1-x}Bi_xSe_2$ ($x \leq 0.4$) revealed that the electrical conductivity of the SbSe$_2$–based compound can be improved by Bi doping,[26] the microscopic origin of the dependence of the transport properties on constituent elements such as pnictogen has been unclear. It is of great importance to investigate what determines the controllability of the carrier concentration and the electrical conductivity in various kinds of the pnictogen dichalcogenide layered compounds.

In this study, we theoretically investigate the electronic and structural properties of several LaOBiS$_2$-type quaternary compounds (LaOBiS$_2$, NdOBiS$_2$, LaOBiSe$_2$, and LaOSbSe$_2$) for undoped and F-doped states using first-principles calculation. Our results suggest that the monoclinic distortion, which is closely related to the *Pn* (*Pn* = Bi, Sb) element, drastically decreases the F-doping capacity. The change in the *Ln* atom from La to Nd in *Ln*OBiS$_2$ makes F doping difficult, which may have some relevance to experimental findings. We also find that the tetragonal structure is gradually stabilized by F doping for all the compounds investigated in this study. The present calculation provides important information on the F-doping capability in the LaOBiS$_2$-type compounds.

This paper is organized as follows. In Sec. II, we outline some computational conditions for crystal structure optimization and calculation of the formation energy of F-doped systems. In Sec. III-A, we demonstrate the electronic and structural properties of compounds that have the same layered structure as LaOBiS$_2$ and different compositions, such as NdOBiS$_2$ and LaOBiSe$_2$, using the first-principles calculation with the generalized gradient approximation (GGA). Subsequently, the feasibility of F-doping in the systems is examined in terms of the formation energy. In Sec. III-B, we demonstrate

the electronic properties of $LaOBiS_2$ and $LaOSbSe_2$ obtained using the first-principles calculation with a hybrid exchange-correlation functional. Their stable structures with and without F-doping are also examined. Finally, we discuss the origin of the different doping abilities of these systems in view of their structural properties. Section IV presents the conclusions.

II. CALCULATION METHOD

A. Structural description and computational conditions for supercell calculations

The $LaOBiS_2$ crystal is composed of alternate stacking of LaO blocking and BiS_2 conducting layers as shown in Fig. 1. Because $LaOBiS_2$ and related compounds were reported to be the tetragonal crystal structure with the $P4/nmm$ space group (No. 129) or the monoclinic structure with the $P2_1/m$ space group (No. 11)[28], we performed the cell-relaxation calculation considering monoclinic as well as tetragonal symmetries in order to elucidate the effect of the crystal symmetry onto the capability of the F-doping.

We utilized the 2×2×1, 2×2×2, 3×3×1, 4×4×1, and √2×√2×1 supercells to deal with systems doped with F at the O sites with the doping concentration x, e.g., $LaO_{1-x}F_xBiS_2$. When one of O atoms in these supercells is replaced by F, x is given as 0.125, 0.0625, 0.0556, 0.03125, and 0.25, respectively. In Sec. III-A, we performed cell relaxation and band structure calculations using the Perdew-Burke-Ernzerhof parameterization of GGA functional[29] for $LaOBiS_2$, $NdOBiS_2$, and $LaOBiSe_2$. In Sec. III-B, we performed these calculations using HSE06 hybrid functional[30] for $LaOSbSe_2$ and $LaOBiS_2$, because we found that $LaOSbSe_2$ becomes metallic in GGA calculation by well-known underestimation of the band gap. Hybrid-functional calculation of $LaOBiS_2$ was performed to compare it with $LaOSbSe_2$. Owing to high computational cost of calculations using the hybrid functional, we used only the unit cell and the √2×√2×1 and 2×2×1 supercells in the analysis of $LaOSbSe_2$ and $LaOBiS_2$ shown in Sec. III-B.

For all the calculations in this paper, we used the projector augmented wave method as implemented in *Vienna ab initio simulation package*.[31-34] In crystal structure optimization, both the atomic coordinates and the cell shapes were optimized with keeping the crystal symmetry. Plane-wave cutoff energy was 550 eV. Brillouin zone sampling was performed by the ***k***-points grid with the following meshes: (12 12 3) for the unit cell; (6 6 3) for the 2×2×1 supercell; (6 6 2) for the 2×2×2 supercell; (4 4 3) for the 3×3×1 supercell; (3 3 3) for the 4×4×1 supercell; and (8 8 3) for the √2×√2×1 supercells. For self-consistent field calculations, the convergence threshold of the total energy was 10^{-7} eV. The ionic relaxation was performed until the Hellmann-Feynman force acting on each atom becomes less than 10^{-2} eV/Å. To represent the strongly localized 4*f* orbitals of Nd atoms, we adopted open-core treatment where $4f^3$ are included into the core. Spin-orbit coupling was not included in this study, the effect of which on the doping capability will be an important future issue.

B. Formation energy of F-doped system

We will discuss how the structural properties influence the doping ability by comparing the formation energy of all the examined compounds. In order to identify the energy stability of F-doped systems, we evaluated the following formation energy:

$$\Delta E_{\mathrm{form}} = E(Ln\mathrm{O}_{1-x}\mathrm{F}_x PnCh_2) + x\mu(\mathrm{O}) - E(Ln\mathrm{O}PnCh_2) - x\mu(\mathrm{F}), \quad (1)$$

where *Ln* = La, Nd, *Pn* = Bi, Sb, and *Ch* = S, Se in this study. Here, $E(A)$ is the total energy that was calculated by assuming a single-crystalline structure of the system. μ(O) and μ(F) denote chemical potentials of O and F, respectively. For simplicity, we assumed $\mu(\mathrm{O})=E(\mathrm{O}_2)/2$ and $\mu(\mathrm{F})= E(\mathrm{F}_2)/2$, which corresponds to the O-rich and F-rich conditions. The way of estimating μ(O) and μ(F) does not affect the following discussion because, in the present study, we aim to examine differences of ΔE_{form} among the compounds rather than the values of ΔE_{form} themselves. In order to obtain $E(\mathrm{O}_2)$ and $E(\mathrm{F}_2)$, we calculated the total energy of the O_2 (F_2) single molecule in the 10 Å×10 Å×10 Å unit cell, where the inter-atom distance was optimized in calculation. We considered spin-polarized state for the O_2 molecule. For calculations of these molecules, we only took the Γ point in the

reciprocal space. We used the same exchange-correlation functional for evaluating all the total energies $E(A)$ in Eq. (1), i.e., GGA in Sec. III-A-3 and HSE06 in Sec. III-B-3. Other computational conditions are the same as those shown in Sec. II-A.

We note that Eq.(1) estimates the difference in total energy between the system before and after the F doping, without considering the charged states. Although the estimation of the defect formation energy generally requires consideration of the charged states of the defect (see Ref. 35, for instance), we used Eq. (1) for simplicity. This can be reasonable for a system where carriers are doped with high concentrations because, in such case, the doped carriers can be regarded as being within the unit cell. Several experimental studies[2,36,37] suggested that substantial electron carriers generated by partial substitution of F for O were doped in the conduction band in La(O,F)BiS_2. Although Eq. (1) is quite simplistic, these experimental results may verify the validity of using it in the present study because we are interested in the stability of systems with relatively high doping concentrations.

Furthermore, although the chemical reaction presented with Eq. (1) is not very realistic, it suffices for our aim of comparing the doping abilities of the compounds, where only the relative values of ΔE are needed. For $LaOSbSe_2$, we also evaluated the energy difference between the non-doped and F-doped systems using more realistic chemical reaction as shown in Sec. III-B-3.

III. RESULTS AND DISCUSSION

A. Comparison of $LaOBiS_2$, $NdOBiS_2$, and $LaOBiSe_2$ using GGA functional

1. *Electronic band structure of mother compounds*

First, we have examined the electronic band structure of $LaOBiS_2$, $NdOBiS_2$, and $LaOBiSe_2$ using first-principles calculation with the GGA functional. The electronic band structures of the undoped systems with the tetragonal structure are shown in Fig. 2. Since all the systems shown here are gapped, we can safely investigate the F-doping effects in the following analysis using GGA.

The electronic band structures of F-doped unitcells—$LaO_{1-x}F_xBiS_2$, $NdO_{1-x}F_xBiS_2$, and $LaO_{1-x}F_xBiSe_2$ with x=0.5—are plotted in Fig. 3. By comparing Fig. 2 and Fig. 3, the addition of F atoms results in *n*-type conductivity without substantially altering the conduction band dispersion around the Fermi level of pure systems even at a high doping level such as x=0.5. Moreover, from local density of states calculation, it has been revealed that the F atoms form deep impurity states over 6 eV lower than the Fermi level. It suggests that the thermoelectric transport calculation under the rigid-band assumption, where the Fermi level is shifted according to the carrier concentration based on the band structure of a pure system, is valid for these compounds. We note that, while the validity of this approximation was already checked for $LaOBiS_2$[38], the present calculation shows that it is valid also for other compounds ($NdOBiS_2$ and $LaOBiSe_2$). Several theoretical studies adopted the rigid band approach to analyze thermoelectric properties (see Ref. 23 and Ref. 39, for instance); the above result assures us that the good performance of $LaOBiS_2$-type materials that was predicted by the previous studies is convincing.

2. *Structural properties of the optimized structure with F-doping*

Figure 4 presents the total energy difference between the monoclinic and tetragonal structures for $LaO_{1-x}F_xBiS_2$, $NdO_{1-x}F_xBiS_2$, and $LaO_{1-x}F_xBiSe_2$ with several values of the doping concentration x. It is noteworthy that the total energy of pure $LaOBiS_2$ is lower for the monoclinic phase with β=91.02° than for the tetragonal phase, which indicates that the stable structure is monoclinic rather than tetragonal. The obtained lattice constants of pure $LaOBiS_2$ (a=4.073 Å, b=4.050 Å, and c=14.295 Å) well reproduce the experimental results (a=4.0769(4) Å, b=4.0618(3) Å, and c=13.885(2) Å; b=90.12(2)°)[28]. This result indicates the validity of the present calculation for examining these systems.

On the other hand, $NdOBiS_2$ and $LaOBiSe_2$ exhibit smaller energy differences between the tetragonal and monoclinic phases than $LaOBiS_2$. For example, the energy difference between the two phases for $NdOBiS_2$ is around 1.2 meV, which is negligibly small, i.e., can be regarded as a numerical error, for the present computational conditions, such as the number of k-points. According to experimental studies, $LaOBiSe_2$ crystallizes in the

tetragonal phase.[40] Furthermore, $NdOBiS_2$ was also reported to be the tetragonal structure.[41-44] The lattice parameters were obtained as $a=b$=4.009 Å and c=14.244 Å for $NdOBiS_2$; $a=b$=4.146 Å and c=14.96 Å for $LaOBiSe_2$ through the cell optimization calculation. The calculation results well reproduced the experimental results: $a=b$=3.98 Å and c=13.56 Å[41] for $NdOBiS_2$ and $a=b$=4.1565(1) Å and c=14.1074(3) Å[40] for $LaOBiSe_2$. Our results are also consistent with the previous theoretical calculation showing that the $P2_1/m$ (monoclinic) and $P4/nmm$ (tetragonal) phases are the most stable for $LaOBiS_2$ and $LaOBiSe_2$, respectively.[45]

However, we note here that the calculated values of c were approximately 3−6% overestimated when compared with the experimental values, in contrast to a and b, where the discrepancies between the calculated and experimental values were within 1%. This overestimation of c might be attributed to the van der Waals interaction between the stacking layers, which is not easy to describe accurately by popular energy functionals.

The dependence of the lattice constants of $LaOBiS_2$ on the doping concentration x is shown in Fig. 5. Here, the crystal symmetry was assumed to be $P2_1/m$ (monoclinic). Our results are consistent with an experimental report,[2] which revealed that the value of c sizably decreases with increasing x. Similarly, F doping for the other two compounds ($NdOBiS_2$ and $LaOBiSe_2$) induced the shrinkage of these cells along the c-axis, which also replicates experimental data[40,44]. Although the magnitudes of c tend to be overestimated, as described above, the good agreement between the theoretical and experimental behaviors after F doping assures us that our analysis is suitable for comparing the stability of F-doped compounds. More interestingly, our results indicate that $LaOBiS_2$ gradually falls into the tetragonal phase by the F-doping, that is, the lattice constants a and b become closer and the angle β approaches 90°. This tendency is also inferred from Fig. 5, where the energy difference between the tetragonal and monoclinic structures vanishes by increasing x.

3. *Formation energy of F-doped systems*

The formation energies ΔE_{form} of the systems doped with F are presented in Fig. 6. The figure contains the calculation results obtained for $LaOBiS_2$, $NdOBiS_2$, and $LaOBiSe_2$ for two different cases: structures optimized assuming the tetragonal and monoclinic phases. For example, a plot for "Tetragonal $LaOBiS_2$" means that we assumed the tetragonal structure when evaluating $E(LaOBiS_2)$ and $E(LaO_{1-x}F_xBiS_2)$ in Eq. (1). Among these compounds, $LaOBiS_2$ has the lowest values of ΔE_{form}, as shown in Fig. 6. This good doping ability agrees with experimental facts[2], which indicates that the electrical properties are easily controlled by doping with F for $LaOBiS_2$. The next lowest ΔE_{form} was obtained for $NdOBiS_2$ and the largest was for $LaOBiSe_2$. That is, the change in chalcogens from S to Se led to a larger increase in ΔE_{form} than the change in lanthanoids from La to Nd. We note that, on the basis of experimental studies that reported successful F-doping into $NdOBiS_2$[41-44] and $LaOBiSe_2$[40,46], the F-doping into all these systems are still possible while the solubility can be different among them.

As shown in Fig. 6, the ΔE_{form} values of monoclinic $LaOBiS_2$ are slightly higher than those of the tetragonal one. This can be understood in terms of structural changes induced by F-doping. As shown in Fig. 6, F-doping decreases the monoclinic distortion of the system; i.e., the system approaches the tetragonal structure. Therefore, in Eq. (1), allowing the monoclinic distortion in calculation mainly lowers $E(LaOBiS_2)$ while a change in $E(LaO_{1-x}F_xBiS_2)$ is smaller. As a result, a higher formation energy is obtained when one allows the monoclinic distortion in calculation. $NdOBiS_2$ and $LaOBiSe_2$ exhibit negligibly small differences between the ΔE_{form} values of the tetragonal and monoclinic phases because the structures of these optimized cells are almost the same as discussed in Sec. III-A-2. We note that, for these systems, the effect of the monoclinic distortion onto the F-doping capability seems to be smaller than that introduced by changing the constituent elements of *Ln* and *Ch*.

Before proceeding to the next section, we point out that the x–ΔE_{form} plots in Fig. 6 exhibit good linearity up to x of 12.5%. In contrast, the plots show nonlinear relationships for larger x. Because calculation of heavily doped systems with sizable interaction among

dopant atoms is challenging owing to the necessity of trying several dopant configurations, we shall focus on x up to 25 % in the remainder of this paper.

B. Comparison of $LaOBiS_2$ and $LaOSbSe_2$ using hybrid functional

1. Electronic band structure of mother compounds

The band structures of the undoped $LaOSbSe_2$ and $LaOBiS_2$ with the tetragonal structure calculated using the HSE06 hybrid functional are shown in Fig. 7. The band dispersion of $LaOBiS_2$ in Fig. 7 (a) closely resembles that obtained using GGA shown in Fig. 2(a). The band dispersion of $LaOSbSe_2$ shown in Fig. 7 (b) is also similar to them, while the band gap is much narrower. In fact, this small band gap ~0.23 eV obtained by HSE06 disappears for GGA because of its well-known underestimation of the band gap, while the experimental study reported the insulating behavior for $LaOSbSe_2$.[24] This is the reason why we adopted HSE06 here rather than GGA.

2. Structural properties of the optimized structure with F-doping

The lattice constants of the pure $LaOBiS_2$ and $LaOSbSe_2$ optimized using HSE06 are listed in Table I. The results show that the monoclinic instability is enhanced in $LaOSbSe_2$ than $LaOBiS_2$, as seen from the large energy difference between the tetragonal and monoclinic phases, the large difference between the lattice constants a and b, and a larger β in monoclinic $LaOSbSe_2$. The energy difference between the tetragonal and monoclinic phases in $LaOBiS_2$ is of the same order of magnitude as that obtained by GGA, which is also listed in Table I. Table I also demonstrates that F-doping reduces the monoclinic distortion for both systems, which is consistent with GGA analysis performed for $LaOBiS_2$ shown in the previous section. We note that, although we obtain a positive total energy of the monoclinic $LaO_{1-x}F_xSbSe_2$ (x = 0.25) relative to that for the tetragonal phase, this might be due to a numerical error since $P2_1/m$ is a subgroup of $P4/nmm$. Nevertheless, we can safely say that the tetragonal structure is actually stabilized by F-doping also for $LaOSbSe_2$ because of the large total energy difference between the two phases for x = 0 and the change in the lattice parameters from x = 0 to

0.25, which suggests that the system falls into (at least closely approaches) the tetragonal phase by F-doping.

According to an experimental work[24], the XRD analysis revealed that $LaOSbSe_2$ has a tetragonal (*P4/nmm* space group) structure with $a = b = 4.14340(3)$ Å and $c = 14.34480(14)$ Å. The calculated lattice constants listed in Table I agree with these experimental values within an error of 3%. We note that, however, the lattice structure determined in this experimental study differs from that predicted in our calculation, to say, the monoclinic lattice. Nevertheless, on the basis of our calculation results that offer reasonable agreement with experimental observation for *Pn* = Bi systems as we have seen in Sec. III-A, we can speculate that a strong instability toward the monoclinic structure should be present in $LaOSbSe_2$. As a matter of fact, some experimental studies reported that $Ce(O,F)Sb(S,Se)_2$, where S:Se = 1:0 or around 1:1, has the monoclinic structure[25,47]. Also in the previous theoretical calculation, replacement of *Pn* atom from Bi to Sb or As tends to stabilize the $P2_1/m$ (monoclinic) phase.[45] Further discussion will be presented in the following section.

3. Formation energy of F-doped systems

The formation energies ΔE_{form} of F-doped $LaOSbSe_2$ and $LaOBiS_2$ are shown in Fig. 8. For calculating the formation energies, we assumed the tetragonal or monoclinic structures just like in Sec. III-A-3. We can see two important features: monoclinic distortion remarkably increases the formation energy for $LaOSbSe_2$, and the tetragonal structures of $LaOSbSe_2$ and $LaOBiS_2$ have rather close values of ΔE_{form}. Since the experimental study reported the tetragonal structure for $LaOSbSe_2$, our calculation results suggest that the capability of F-doping is not so different between $LaOBiS_2$ and $LaOSbSe_2$. In fact, the experimental observation that the F doping induced some change of the transport properties in $LaOSbSe_2$[24] suggests that F atoms are indeed doped in the system although the system remains insulating. Our calculation suggests that the structural instability in tetragonal $LaOSbSe_2$ can play some role in its insulating behavior through the local structural distortion leading to the difficulty in F-doping. It is also

noteworthy that the monoclinic distortion in *Ln*O*PnCh*$_2$ results in the deformation of the conducting layer from the two-dimensional square lattice to the (quasi-)one-dimensional chains[28] (Fig. 9), where the transport should be more easily disturbed by several scattering processes due to its low dimensionality.

While the formation energies calculated so far in this paper are all negative, this does not necessarily indicate that this impurity doping was achieved without any hindrance because of our simple treatment of F-doping. For example, the chemical reaction used in Eq. (1) is clearly different from the actual synthesis. Whereas our analysis should be sufficient to roughly see the material dependence of the F-doping capability and the strength of the monoclinic distortion, we here evaluated ΔE_{form} based on a more practical chemical reaction for $LaOSbSe_2$. In its experimental synthesis, La_2O_3, Sb_2Se_3, LaSe, $LaSe_2$, and LaF_3 were used.[24] Using these precursors, we evaluated the total energies before and after synthesizing $LaO_{1-x}F_xSbSe_2$ as follows:

$$\frac{1-x}{3}E(\mathrm{La_2O_3}) + \frac{1}{8}E(\mathrm{Sb_2Se_3}) + \frac{1+4x}{24}E(\mathrm{LaSe}) + \frac{1-2x}{24}E(\mathrm{LaSe_2}) + \frac{x}{18}E(\mathrm{LaF_3})$$
$$\rightarrow E(\mathrm{LaO_{1-x}F_xSbSe_2}). \qquad (2)$$

Thus, by taking the difference between the left-hand side with a finite x and that for $x = 0$, the capability of the F-doping into $LaOSbSe_2$ can be evaluated by the following energy difference,

$$E(\mathrm{LaO_{1-x}F_xSbSe_2})$$
$$-\left[E(\mathrm{LaOSbSe_2}) - \frac{x}{3}E(\mathrm{La_2O_3}) + \frac{x}{6}E(\mathrm{LaSe}) - \frac{x}{12}E(\mathrm{LaSe_2}) + \frac{x}{18}E(\mathrm{LaF_3})\right]. \qquad (3)$$

We computed Eq. (3) and obtained the values of 0.42 eV and 0.64 eV for tetragonal and monoclinic $LaO_{0.75}F_{0.25}SbSe_2$, respectively. This suggests that the F-doping into $LaOSbSe_2$ seems difficult, at least for relatively large $x = 0.25$. More careful analysis on a dilute F-doped system would be an important future study.

IV. CONCLUSIONS

We have theoretically investigated the structural properties of *Ln*O*PnCh*$_2$-type quaternary compounds ($LaOBiS_2$, $NdOBiS_2$, $LaOBiSe_2$, and $LaOSbSe_2$) and examined

their influences on F doping. Our results show that replacement of atoms from La to Nd and S to Se in $LaOBiS_2$ crystal makes F doping difficult, which may have some relevance to experimental observation. We also find that replacement of the *Pn* element from Bi to Sb increases the monoclinic distortion of the mother compound and, in consequence, decreases the capability of F doping. That is, large formation energy is necessary for doping the monoclinic $LaOSbSe_2$ with F owing to the monoclinic-to-tetragonal transformation induced by F doping. Therefore, it is suggested that the difficulty in controlling the electrical properties of $LaOSbSe_2$ by F doping, which was experimentally observed, is partly attributed to its low doping ability related to the predisposition towards distortion. Our theoretical work can provide important information on carrier density control in *Ln*O*PnCh*$_2$ systems.

Although the present paper focuses on the substitutional doping of F in the O site as the primary structure of F-doped $LaOBiS_2$-type compounds, it would be important to discuss the possibility of occupying the interstitial site in future studies. If this occurs, the interstitial F atoms can be charged as F^-, which results in unintentional hole doping. In addition, intrinsic charged defects of the parent compounds can be formed and affect the carrier concentration. Thus, these defects could be associated with the low electrical conductivity of $LaOSbSe_2$. Further studies are necessary to clarify this point.

ACKNOWLEDGEMENT

We appreciate the fruitful discussions with Professor Yoshikazu Mizuguchi and Professor Yosuke Goto. This work was supported by JSPS KAKENHI (Grant No. JP17H05481 and Grant No. JP19H04697) and JST CREST (Grant No. JPMJCR16Q6), Japan. A part of the computation in this work has been done using the facilities of the Supercomputer Center, the Institute for Solid State Physics, the University of Tokyo.

REFERENCES

1. Y. Mizuguchi, J. Phys. Soc. Jpn **88**, 041001 (2019).

2. Y. Mizuguchi, S. Demura, K. Deguchi, Y. Takano, H. Fujihisa, Y. Gotoh, H. Izawa, and O. Miura, J. Phys. Soc. Jpn. **81**, 114725 (2012).

3. K. Deguchi, Y. Takano, and Y. Mizuguchi, Sci. Technol. Adv. Mater. **13**, 054303 (2012).

4. Y. Mizuguchi, Physics Procedia **58**, 94 (2014).

5. Y. Mizuguchi, J. Phys. Chem. Solids **84**, 34 (2015).

6. D. Yazici, I. Jeon, B.D. White, M.B. Maple, Physica C **514**, 218 (2015)

7. H. Usui and K. Kuroki, Novel Supercond. Mater. **1**, 50 (2015).

8. Y. Mizuguchi, Condens. Matter **2**, 6 (2017).

9. N. Kase, K. Kondo, M. Koike, S. Watanabe, and N. Miyakawa, AIP Advances **8**, 101322 (2018).

10. K. Suzuki, H. Usui, K. Kuroki, T. Nomoto, K. Hattori, and H. Ikeda, J. Phys. Soc. Jpn. **88**, 041008 (2019).

11. A. Omachi, J. Kajitani, T. Hiroi, O. Miura, and Y. Mizuguchi, J. Appl. Phys. **115**, 083909 (2014).

12. I. Pallecchi, G. Lamura, M. Putti, J. Kajitani, Y. Mizuguchi, O. Miura, S. Demura, K. Deguchi, and Y. Takano, Phys. Rev. B **89**, 214513 (2014).

13. Y. Mizuguchi, A. Miura, A. Nishida, O. Miura, K. Tadanaga, N. Kumada, C. H. Lee, E. Magome, C. Moriyoshi, Y. Kuroiwa, J. Appl. Phys. **119**, 155103 (2016)

14. A. Nishida, H. Nishiate, C. H. Lee, O. Miura, Y. Mizuguchi, J. Phys. Soc. Jpn. **85**, 074702 (2016)

15. C. H. Lee, A. Nishida, T. Hasegawa, H. Nishiate, H. Kunioka, S. Ohira-Kawamura, M. Nakamura, K. Nakajima, and Y. Mizuguchi, Appl. Phys. Lett. **112**, 023903 (2018)

16. Y. Mizuguchi, A Nishida, A Omachi, O Miura, Cog. Phys. **3**, 1156281 (2016).

17. C-H. Lee, J. Phys. Soc. Jpn **88**, 041009 (2019).

18. M. Ochi, H. Usui, and K. Kuroki, J. Phys. Soc. Jpn **88**, 041010 (2019).

19. Y. Mizuguchi, A. Omachi, Y. Goto, Y. Kamihara, M. Matoba, T. Hiroi, J. Kajitani, O. Miura, J. Appl. Phys. **116**, 163915 (2014).

20. K. Terashima, J. Sonoyama, T. Wakita, M. Sunagawa, K. Ono, H. Kumigashira, T. Muro, M. Nagao, S. Watauchi, I. Tanaka, H. Okazaki, Y. Takano, O. Miura, Y. Mizuguchi, H. Usui, K. Suzuki, K. Kuroki, Y. Muraoka, T. Yokoya, Phys. Rev. B **90**, 220512(R) (2014)

21. A. Miura, Y. Mizuguchi, T. Takei, N. Kumada, E. Magome, C. Moriyoshi, Y. Kuroiwa, K. Tadanaga, Solid State Commun. **227**, 19 (2016).

22. A. Nishida, O. Miura, C. H. Lee, and Y. Mizuguchi, Appl. Phys. Exp. **8**, 111801 (2015).

23. M. Ochi, H. Usui, and K. Kuroki, Phys. Rev. Appl. **8**, 064020 (2017).

24. Y. Goto, A. Miura, R. Sakagami, Y. Kamihara, C. Moriyoshi, Y. Kuroiwa, and Y. Mizuguchi, J. Phys. Soc. Jpn. **87**, 074703 (2018).

25. M. Nagao, M. Tanaka, R. Matsumoto, H. Tanaka, S. Watauchi, Y. Takano, I. Tanaka, Cryst. Growth Des. **16**, 3037 (2016).

26. Y. Goto, A. Miura, C. Moriyoshi, Y. Kuroiwa, and Y. Mizuguchi, J. Phys. Soc. Jpn. **88**, 024705 (2019).

27. K. Momma and F. Izumi, J. Appl. Crystallogr. **44**, 1272 (2011).

28. R. Sagayama, H. Sagayama, R. Kumai, Y. Murakami, T. Asano, J. Kajitani, R. Higashinaka, T. D. Matsuda, and Y. Aoki, J. Phys. Soc. Jpn. **84**, 123703 (2015).

29. J. P. Perdew, K. Burke, and M. Ernzerhof, Phys. Rev. Lett. **77**, 3865 (1996).

30. A. V. Krukau, O. A. Vydrov, A. F. Izmaylov, and G. E. Scuseria, J. Chem. Phys. **125**, 224106 (2006).

31. G. Kresse and J. Hafner, Phys. Rev. B **47**, 558(R) (1993).

32. G. Kresse and J. Hafner, Phys. Rev. B **49**, 14251 (1994).

33. G. Kresse and J. Furthmu□ller, Comput. Mater. Sci. **6**, 15 (1996).

34. G. Kresse and J. Furthmu□ller, Phys. Rev. B **54**, 11169 (1996).

35. S. Lany and A. Zunger, Phys. Rev. B **78**, 235104 (2008).

36. Y. Y. Chin, H.-J. Lin, Z. Hu, M. Nagao, Y. Du, X. Wan, B. -J. Su, L. Y. Jang, T. S. Chan, H. -Y. Chen, Y. L. Soo, and C. T. Chen, Phys. Rev. B **94**, 035150 (2016).

37. S. Nagira, J. Sonoyama, T. Wakita, M. Sunagawa, Y. Izumi, T. Muro, H. Kumigashira, M. Oshima, K. Deguchi, H. Okazaki, Y. Takano, O. Miura, Y. Mizuguchi, K. Suzuki, H. Usui, K. Kuroki, K. Okada, Y. Muraoka, and T. Yokoya, J. Phys. Soc. Jpn. **83**, 033703 (2014).

38. B. Li, Z. W. Xing, and G. Q. Huang, Europhys. Lett. **101**, 47002 (2013).

39. G. Wang, D. Wang, X. Shi and Y. Peng, Mod. Phys. Lett. B **31**, 1750265 (2017).

40. S. L. Wu, Z. A. Sun, F. K. Chiang, C. Ma, H. F. Tian, R. X. Zhang, B. Zhang, J. Q. Li, and H. X. Yang, Solid State Commun. **205**, 14 (2015).

41. V. S. Tanryverdiev, O. M. Aliev, and I. I. Aliev, Inorganic Materials **31**, 1497 (1995).

42. D. Yazici, K. Huang, B. D. White, A. H. Chang, A. J. Eriedman, and M. B. Maple, Philos. Mag. **93**, 673 (2012).

43. M. Nagao, S. Demura, K. Deguchi, A. Miura, S. Watauchi, T. Takei, Y. Takano, N. Kumada, and I. Tanaka, J. Phys. Soc. Jpn. **82**, 113701 (2013).

44. S. Demura, Y. Mizuguchi, K. Deguchi, H. Okazaki, H. Hara, T. Watanabe, S. J.

Denholme, M. Fujioka, T. Ozaki, H. Fujihisa, Y. Gotoh, O. Miura, T. Yamaguchi, H. Takeya, and Y. Takano, J. Phys. Soc. Jpn. **82**, 033708 (2013).

45. Q. Liu, X. Zhang, and A. Zunger, Phys. Rev. B **93**, 174119 (2016).

46. M. Nagao, M. Tanaka, S. Watauchi, I. Tanaka, and Y. Takano, J. Phys. Soc. Jpn. **83**, 114709 (2014).

47. M. Nagao, M. Tanaka, A. Miura, M. Kitamura, K. Horiba, S. Watauchi, Y. Takano, H. Kumigashira, and I. Tanaka, Solid State Commun. **289**, 38 (2019).

Table I. Calculated total energies and lattice constants of $LaO_{1-x}F_xBiS_2$ and $LaO_{1-x}F_xSbSe_2$ for x = 0 and 0.25. Total energy relative to that for the tetragonal structure is shown for the monoclinic structure.

Material (functional)	Doping concentration x	Structure	Total energy (eV/cell)	a (Å)	b (Å)	c (Å)	β
$LaOBiS_2$ (hybrid)	x=0	Tetragonal	−	4.026	4.026	14.15	90°
		Monoclinic	−0.03	4.065	4.025	14.19	91.2°
	x=0.25	Tetragonal	−	4.038	4.038	13.74	90°
		Monoclinic	−0.01	4.046	4.046	13.69	90.3°
$LaOBiS_2$ (GGA)	x=0	Tetragonal	−	4.050	4.050	14.25	90°
		Monoclinic	−0.01	4.073	4.050	14.30	91.0°
	x=0.25	Tetragonal	−	4.066	4.066	13.81	90°
		Monoclinic	0.00	4.066	4.066	13.81	90.0°
$LaOSbSe_2$ (hybrid)	x=0	Tetragonal	−	4.071	4.071	14.59	90°
		Monoclinic	−0.18	4.157	4.062	14.76	92.0°
	x=0.25	Tetragonal	−	4.118	4.118	13.85	90°
		Monoclinic	0.04	4.117	4.117	14.09	90.2°

FIG. 1. (a) Crystallographic structure of *Ln*O*PnCh*$_2$, which consists of alternate stacking of *Ln*O blocking and *PnCh*$_2$ conduction layers. Here, the *Ln* (green), O (red), *Pn* (purple), and *Ch* (yellow) atoms are displayed. (b) Unit cell shown with the lattice parameters. The lattice parameters follow the conditions $a = b \neq c$ and $\alpha = \beta = \gamma = 90°$ for the tetragonal (*P*4/*nmm* space group) structure and $a \neq b \neq c$ and $\beta \neq 90°$ for the monoclinic ($P2_1/m$ space group) structure. Depicted using the VESTA software.[27]

(a)

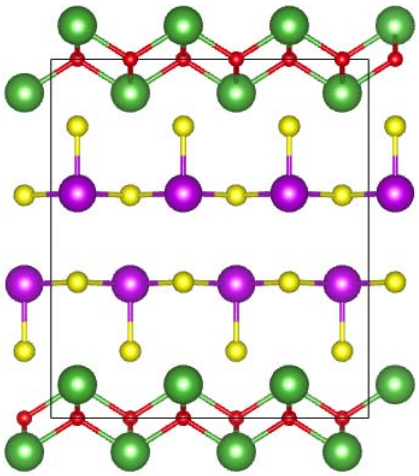

(b)

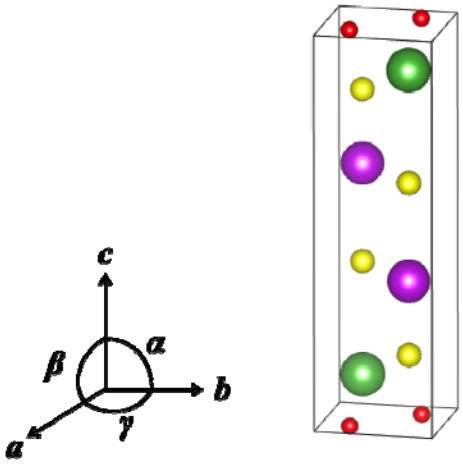

FIG. 2. Electronic band structures of tetragonal (a) $LaOBiS_2$, (b) $NdOBiS_2$, and (c) $LaOBiSe_2$ crystals obtained using the first-principles calculation with the GGA functional.

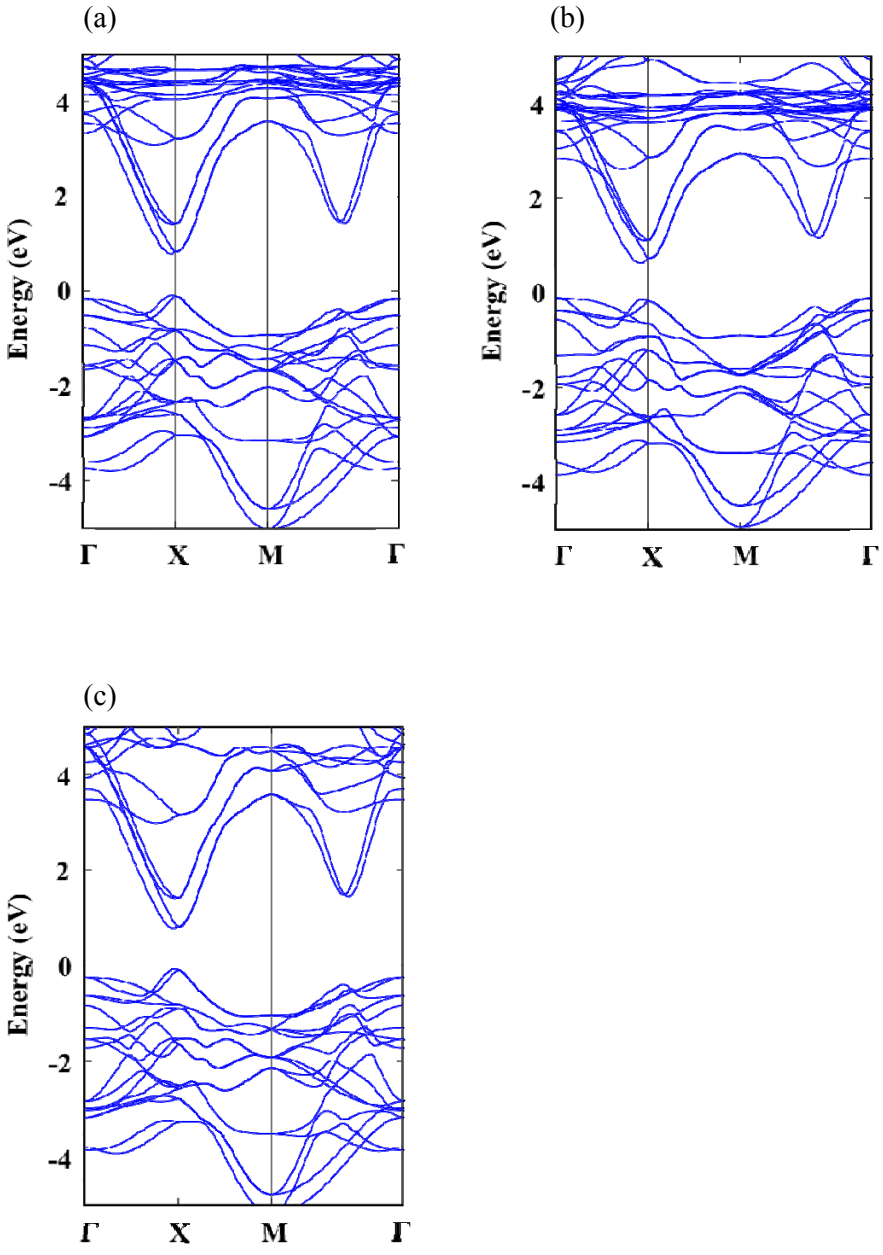

FIG. 3. Electronic band structures of tetragonal (a) $LaO_{1-x}F_xBiS_2$, (b) $NdO_{1-x}F_xBiS_2$, and (c) $LaO_{1-x}F_xBiSe_2$ crystals with x=0.5, obtained from first-principles calculation with the GGA functional. The Fermi level is set to the origin of the energy axis.

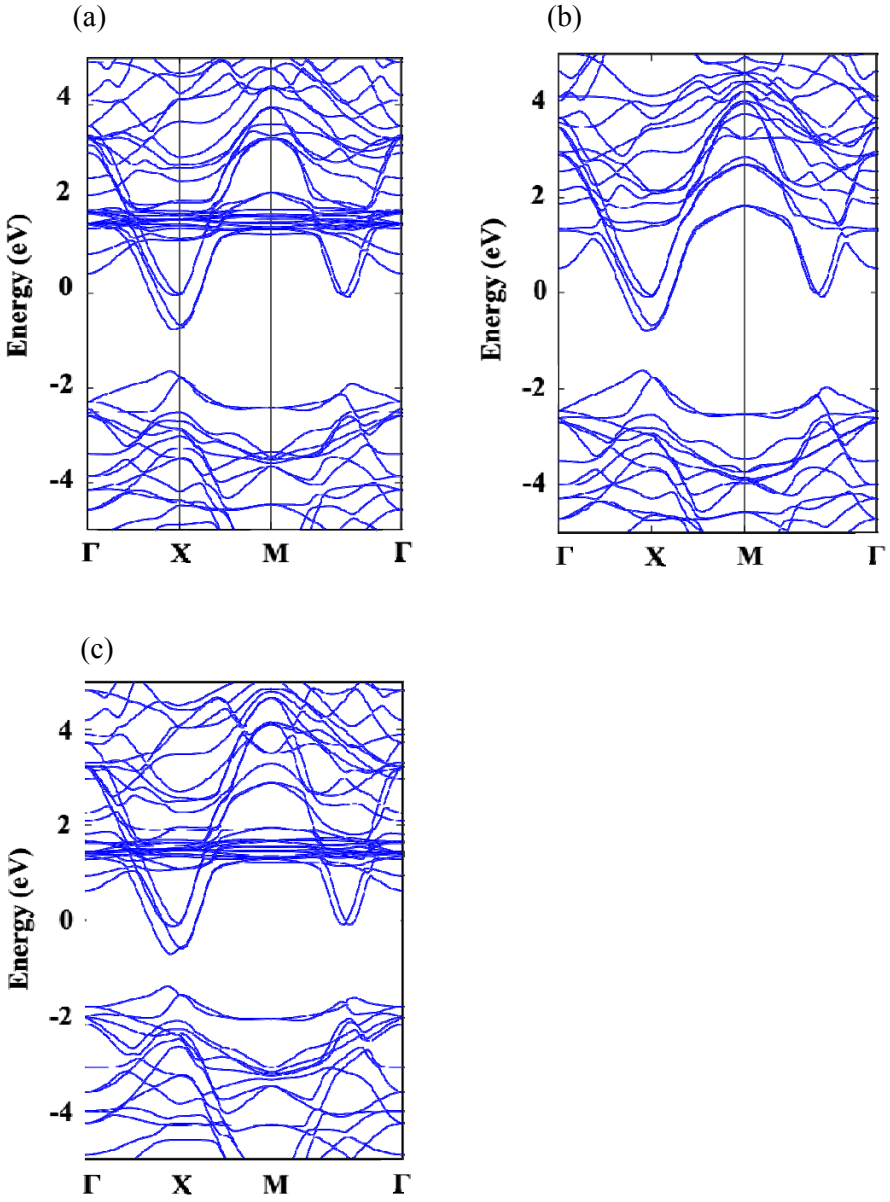

FIG. 4. Total energy difference between the monoclinic and tetragonal structures for $LaO_{1-x}F_xBiS_2$ (circles), $NdO_{1-x}F_xBiSe_2$ (triangles), and $LaO_{1-x}F_xBiSe_2$ (squares), calculated using GGA.

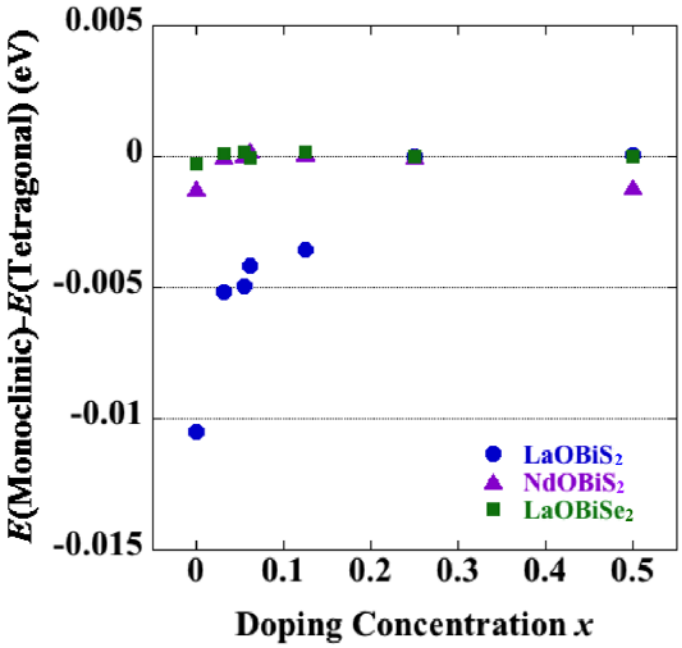

FIG. 5. Dependences of the lattice constants (a) *a*, *b*, *c*, and (b) β on the F doping concentration *x* for the optimized structures of $LaO_{1-x}F_xBiS_2$.

(a)

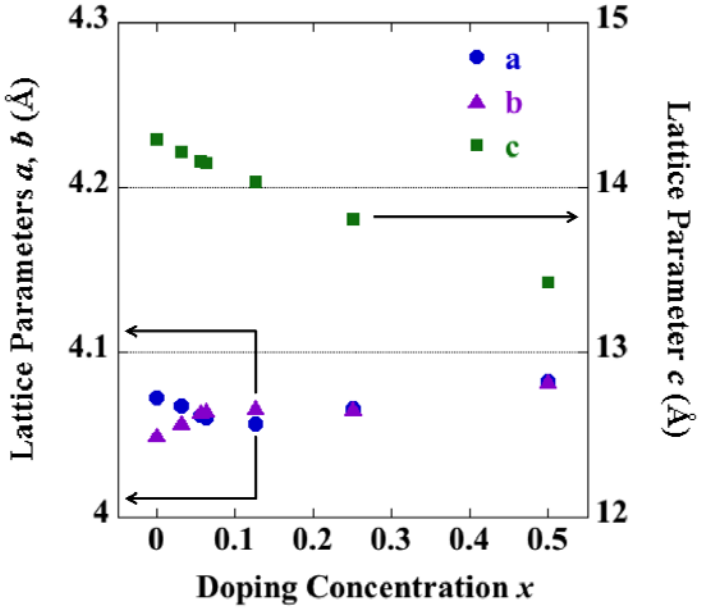

(b)

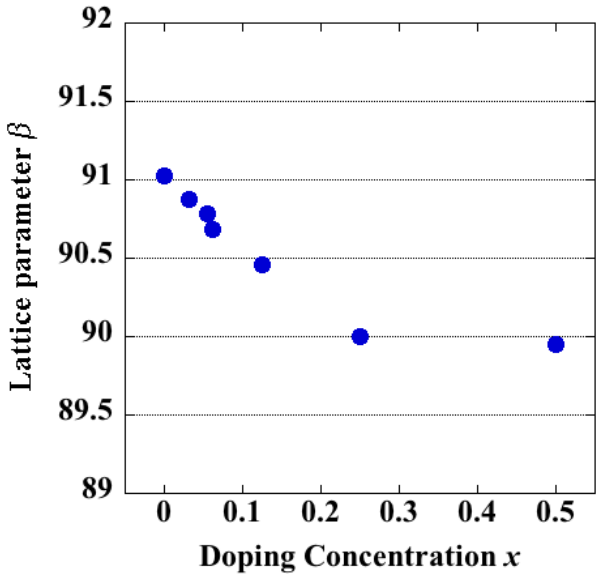

FIG. 6. Dependency of the formation energy ΔE_{form} on the F doping concentration x for $LaO_{1-x}F_xBiS_2$, $NdO_{1-x}F_xBiS_2$, and $LaO_{1-x}F_xBiSe_2$, calculated using GGA. The plot shows each compound with the tetragonal (solid symbols) and monoclinic crystallographic (open symbols) structures.

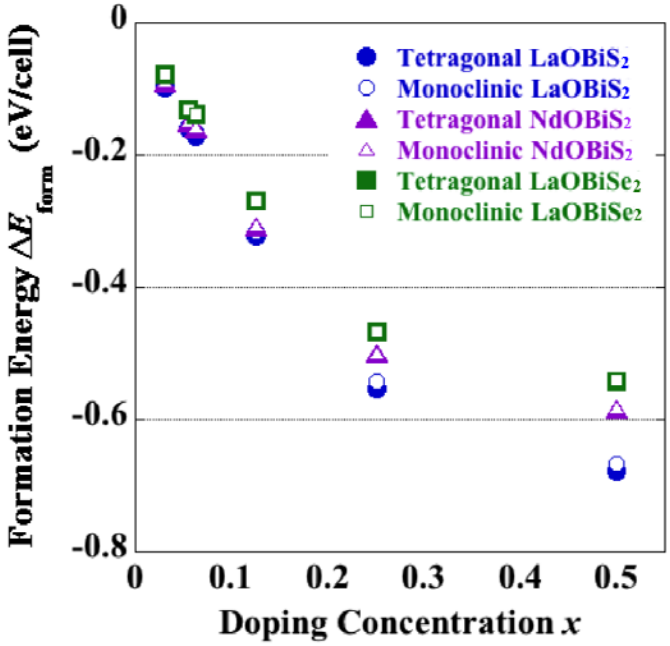

FIG. 7. Electronic band structures of (a) $LaOBiS_2$ and (b) $LaOSbSe_2$ for the tetragonal structure obtained using the HSE06 hybrid functional.

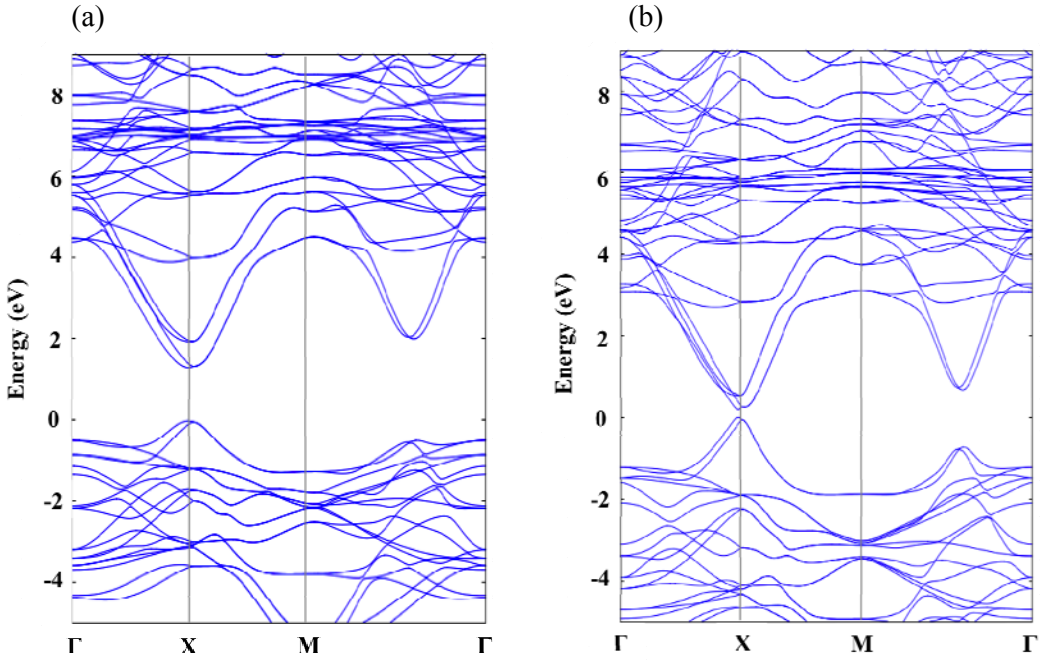

FIG. 8. Dependency of the formation energy ΔE_{form} on the F doping concentration x for $LaO_{1-x}F_xBiS_2$ and $LaO_{1-x}F_xSbSe_2$, calculated using the HSE06 hybrid functional. The graph contains different crystallographic structures for each compound, the tetragonal (solid symbols) and monoclinic (open symbols) structures. For the monoclinic structure, only the case of x=0.25 is shown.

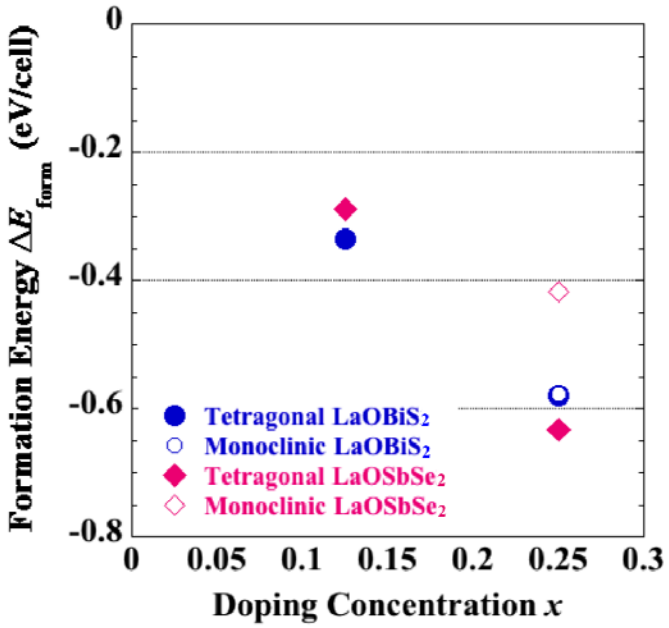

FIG 9. The $SbSe_2$ conductive layer in $LaOSbSe_2$ crystal structures optimized assuming (left) the tetragonal and (right) the monoclinic phases. The bonds are displayed between the nearest Sb and Se atoms that are separated by a distance of 3 Å or less.